

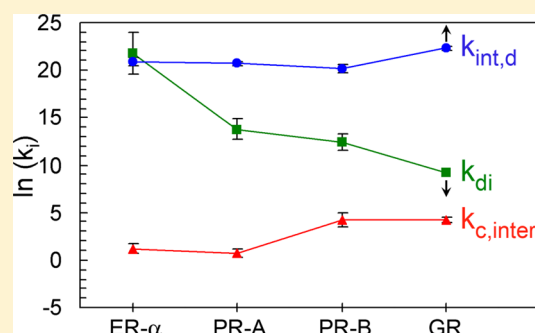
# Glucocorticoid Receptor–Promoter Interactions: Energetic Dissection Suggests a Framework for the Specificity of Steroid Receptor-Mediated Gene Regulation

James P. Robblee, Michael T. Miura, and David L. Bain\*

Department of Pharmaceutical Sciences, University of Colorado Anschutz Medical Campus, 12850 East Montview Boulevard, Aurora, Colorado 80045, United States

## S Supporting Information

**ABSTRACT:** The glucocorticoid receptor (GR) is a member of the steroid receptor family of ligand-activated transcription factors. A number of studies have shown that steroid receptors regulate distinct but overlapping sets of genes; however, the molecular basis for such specificity remains unclear. Previous work from our laboratory has demonstrated that under identical solution conditions, three other steroid receptors [the progesterone receptor A isoform (PR-A), the progesterone receptor B isoform (PR-B), and estrogen receptor  $\alpha$  (ER- $\alpha$ )] differentially partition their self-association and promoter binding energetics. For example, PR-A and PR-B generate similar dimerization free energies but differ significantly in their extents of intersite cooperativity. Conversely, ER- $\alpha$  maintains an intersite cooperativity most comparable to that of PR-A yet dimerizes with an affinity orders of magnitude greater than that of either of the PR isoforms. We have speculated that these differences serve to generate receptor-specific promoter occupancies, and thus receptor-specific gene regulation. Noting that GR regulates a unique subset of genes relative to the other receptors, we hypothesized that the receptor should maintain a unique set of interaction energetics. We rigorously determined the self-association and promoter binding energetics of full-length, human GR under conditions identical to those used in our earlier studies. We find that unlike all other receptors, GR shows no evidence of reversible self-association. Moreover, GR assembles with strong intersite cooperativity comparable to that seen only for PR-B. Finally, simulations show that such partitioning of interaction energetics allows for receptor-specific promoter occupancies, even under conditions where multiple receptors are competing for binding at identical sites.



The glucocorticoid receptor (GR) is a member of the steroid receptor family of ligand-activated transcription factors.<sup>1</sup> The remaining members include the androgen receptor (AR), the mineralocorticoid receptor (MR), the two isoforms of the progesterone receptor (PR-A and PR-B), and the two isoforms of the estrogen receptor (ER- $\alpha$  and ER- $\beta$ ). The domain structure of GR is shown in Figure 1A. GR has a highly conserved DNA binding domain (DBD), a modestly conserved hormone binding domain (HBD), and a poorly conserved N-terminal region (NTR). Located within the N-terminal region and the HBD are transactivation functions AF-1 and AF-2, respectively.

The biochemical understanding of steroid receptor action is as follows: ligand-bound receptors dimerize, assemble at palindromic response elements typically located upstream of a transcriptional start site, and then recruit coactivator proteins to initiate transcription. This model nonetheless remains incomplete. For example, all steroid receptors bind identical or nearly identical DNA response elements *in vitro* yet activate distinct but overlapping sets of genes *in vivo*.<sup>2–4</sup> How then does an individual receptor maintain the specificity of gene control, the ability to activate only a subset of potential genes,

and how does this occur when multiple types of receptors may be present and thus competing for binding at identical response elements? We are focused on determining the quantitative mechanisms responsible for such promoter- and receptor-specific gene regulation.

Shown in Figure 1B are the assembly states and interaction parameters for binding of the receptor to a single palindromic response element. Receptors may dimerize in the absence of DNA ( $k_{di}$ ) and then bind as preformed dimers ( $k_{int,d}$ ) or bind as successive monomers ( $k_{int,m}$ ) via DNA-induced intrasite cooperativity ( $k_{c,intra}$ ). These events each constitute a microscopic interaction, whereas the total binding affinity ( $K_{tot}$ ) describes the macroscopic reaction for two monomers assembling at a response element regardless of pathway. Finally, shown in Figure 1C is the fully ligated state for a promoter containing two hormone response elements. Complete occupancy of receptor dimers at the promoter may be accompanied by intersite cooperativity ( $k_{c,inter}$ ). We note that

Received: March 27, 2012

Revised: May 11, 2012

Published: May 15, 2012



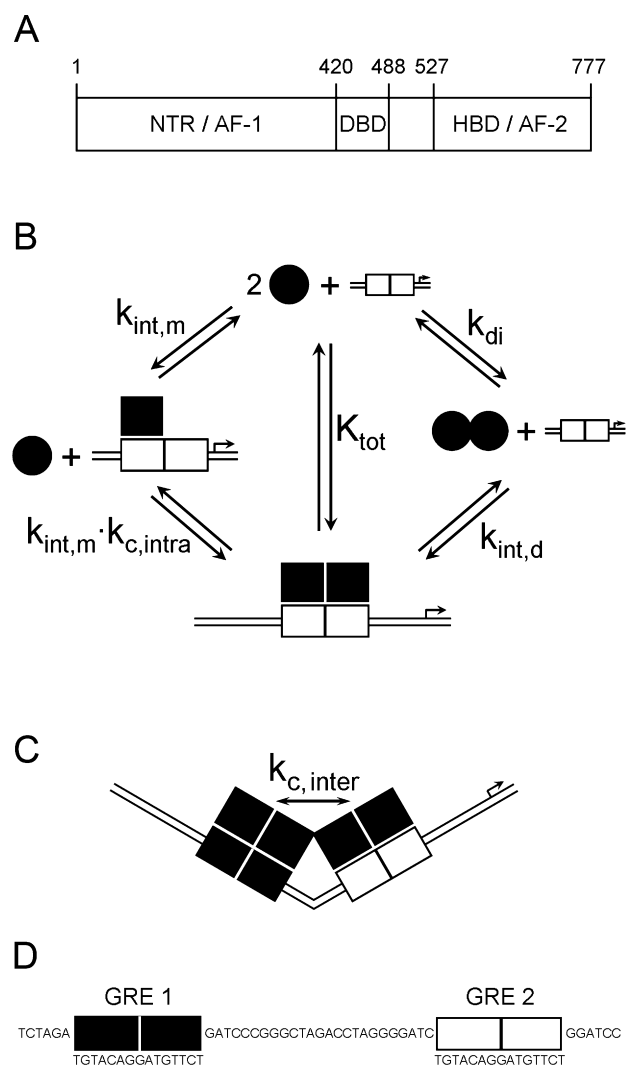


**Figure 1.** GR domain structure and promoter assembly states. (A) Schematic of the GR primary sequence with the domains labeled as follows: NTR, N-terminal region; DBD, DNA binding domain; HBD, hormone binding domain. Activation functions (AF-1 and AF-2) are contained within the NTR and HBD, respectively. (B) Schematic describing binding models for assembly onto a palindromic response element. Filled circles represent GR monomers. Filled squares represent GR dimers. The series of reactions to the left describe a monomer binding pathway, whereby GR monomers assemble sequentially at the response element. The first GR monomer binds with a monomer intrinsic affinity,  $k_{\text{int},m}$ , whereas the second monomer binding event is described by  $k_{\text{int},m}$  and a cooperative interaction between adjacently bound GR monomers ( $k_{\text{c},\text{intra}}$ ). The center reaction describes the total binding affinity ( $K_{\text{tot}}$ ) for saturating a single response element with two GR monomers. The series of reactions to the right describe a dimer binding pathway, whereby GR solution dimerization ( $k_{\text{di}}$ ) precedes binding of the dimer to a response element ( $k_{\text{int},d}$ ). (C) Schematic describing the GR binding assembly at a two-site promoter. All binding constants described in panel B apply at each site on the promoter. Additionally, saturation of both promoter sites may be accompanied by an intersite cooperative interaction ( $k_{\text{c},\text{inter}}$ ), which is depicted by protein–protein contacts between adjacently bound GR proteins and bending of the DNA. (D) Sequence of the GRE<sub>2</sub> promoter sequence proximal to the two response element binding sites, with each half-site underlined.

all of these parameters, including the total binding affinity, have a precise molecular interpretation. By contrast, an apparent

binding affinity, the parameter historically measured in nearly all steroid receptor–DNA binding studies, is a composite of some or all of these values and thus offers little molecular insight.

We previously dissected the microscopic energetics of binding of PR-A and PR-B to the promoter in Figure 1D consisting of two palindromic response elements.<sup>5,6</sup> Under identical conditions, the two isoforms bind the promoter with similar apparent binding affinities; however, the microstate energetics are dramatically different. In particular, the B isoform generates significantly increased intersite cooperativity ( $k_{\text{c},\text{inter}}$ ) relative to that of PR-A. We subsequently found that differences in microstate energetics applied not just to different isoforms but also to different receptors. Under conditions identical to our work on the PR isoforms, we found that ER- $\alpha$  maintained intersite cooperative energetics that were much weaker than those of either PR-A or PR-B, but dimerization energetics that were greater by orders of magnitude.<sup>7</sup>

These studies demonstrated that homologous transcription factors were capable of differentially partitioning their microscopic interaction energetics. This led us to speculate that such differences might serve to generate receptor-specific promoter occupancy and thus receptor-specific gene regulation. For example, if multiple receptors are present at identical total concentrations, stronger dimerization energetics by one (e.g., ER- $\alpha$ ) will generate a greater concentration of active dimers. Consequently, promoter layouts containing an abundance of palindromic response elements should allow preferential binding by that receptor over all others. By contrast, promoters containing a higher proportion of half-site response elements should generate preferential monomer binding by that subset of receptors with weak dimerization energetics (e.g., PR-A and PR-B). Receptor-specific differences in intersite cooperativity should serve as an additional mechanism for controlling receptor-specific promoter occupancy.<sup>5</sup>

As a step toward determining whether such a framework might be generalized to all members of the steroid receptor family, we dissected the energetics of binding of GR to the promoter in Figure 1D (herein defined as GRE<sub>2</sub>). We hypothesized that GR, which regulates a unique subset of genes relative to the PR isoforms,<sup>4</sup> should maintain a unique set of microstate interaction parameters. Consistent with this hypothesis, we found that GR dimerization energetics are considerably weaker than those of any of the other receptors, including PR-A and PR-B. In fact, we were unable to detect reversible GR self-association regardless of protein concentration. Furthermore, although GR intersite cooperativity is comparable to that of PR-B, it is much greater than that of PR-A and ER- $\alpha$ . Simulations reveal that such unique partitioning of microstate energetics allows for receptor-specific promoter occupancy, even in the presence of competitive binding by another receptor. Our results thus suggest that the ability of homologous receptors to differentially partition their microscopic energetics may serve as the basis for receptor-specific and promoter-specific gene control.

## MATERIALS AND METHODS

**Expression and Purification of Full-Length Human GR.** A pBAC baculovirus vector (EMD, formerly Novagen) containing human GR (amino acids 1–777) fused to an N-terminal hexahistidine tag (His-GR) was generated in house. A vector containing human GR fused to an N-terminal FLAG tag (FLAG-GR) was donated by S. Nordeen (University of

Colorado Anschutz Medical Campus). Both constructs were expressed in baculovirus-infected Sf9 cells using a multiplicity of infection of 1. Cells were treated with 1  $\mu$ M triamcinolone acetonide (TA) 24 h postinfection and harvested 24 h later.

All purification steps were conducted at 4 °C in the presence of 10  $\mu$ M TA. Cells containing His-GR were Dounce homogenized in a buffer containing 20 mM Tris (pH 8.0 at 4 °C), 10% glycerol (w/v), 10 mM NaCl, 10 mM  $\beta$ -ME, 10  $\mu$ M TA, and protease inhibitors (Complete, EDTA-free, Roche). The nuclear-localized fraction of His-GR was pelleted, and the receptor was released from the nuclei in an extraction buffer containing 20 mM Tris (pH 8.0 at 4 °C), 10% glycerol (w/v), 500 mM NaCl, 10 mM  $\beta$ -ME, 10  $\mu$ M TA, 25 mM imidazole, and protease inhibitors. Following centrifugation, His-GR was purified from the supernatant using Ni-NTA agarose resin (Qiagen). The resin was washed extensively with extraction buffer, and the receptor was eluted using the same buffer now containing 250 mM imidazole. His-GR then was chromatographed on a Sephacryl S-300 HR size exclusion column (GE Healthcare) equilibrated in the extraction buffer without imidazole and protease inhibitors. The fractionated protein was dialyzed into 20 mM Tris (pH 8.0 at 4 °C), 10% glycerol (w/v), 85 mM NaCl, 10 mM  $\beta$ -ME, and 10  $\mu$ M TA and concentrated using Q-Sepharose (Amersham Biosciences). After elution with a 500 mM NaCl step gradient, His-GR was flash-frozen and stored in liquid nitrogen. The receptor was judged to be approximately 95% pure by quantification of Coomassie Blue-stained sodium dodecyl sulfate–polyacrylamide gel electrophoresis (SDS–PAGE) gels. Concentrations were determined using a calculated extinction coefficient of 71280 M<sup>-1</sup> cm<sup>-1</sup>.<sup>8</sup> Final yields were 0.3–0.5 mg of His-GR/L of cell culture.

FLAG-GR was purified as described for His-GR with the following modifications. After the initial pelleting step, FLAG-GR was extracted from the nuclei using the previously described extraction buffer without imidazole. After centrifugation, the receptor was partially purified from the supernatant using Anti-FLAG M2 Affinity Gel (Sigma). The resin was washed extensively, and the receptor was eluted using 0.25 mg/mL FLAG peptide (Sigma). The eluted receptor was then chromatographed and concentrated as described for His-GR. FLAG-GR was judged to be approximately 95% pure by quantification of Coomassie Blue-stained SDS–PAGE gels. The FLAG-GR concentration was determined using a calculated extinction coefficient of 72270 M<sup>-1</sup> cm<sup>-1</sup>.<sup>8</sup> Final yields were comparable to those of His-GR.

**Analytical Ultracentrifugation.** All sedimentation analyses were conducted on a Beckman XL-A analytical ultracentrifuge equipped with absorbance optics and an An-50 Ti rotor. Two- and six-channel Epon centerpiece-containing cells were used for sedimentation velocity and sedimentation equilibrium experiments, respectively. All studies were conducted in a buffer containing 20 mM Tris (pH 8.0 at 4 °C), 100 mM NaCl, 1 mM DTT, 1 mM CaCl<sub>2</sub>, 2.5 mM MgCl<sub>2</sub>, and 10  $\mu$ M TA.

For sedimentation velocity, three GR samples at 10.0, 5.0, and 2.0  $\mu$ M were sedimented at 4 °C using a rotor speed of 50000 rpm. Data were collected at 280 nm, with scans taken as quickly as the instrument would allow (typically every 4 min). Sedimentation coefficient distributions [ $c(s)$ ] were calculated using Sedfit.<sup>9</sup> The  $c(s)$  distribution was corrected to 20 °C and water ( $s_{20,w}$ ) using standard methods,<sup>10</sup> where  $s_{20,w}$  is defined as

$$s_{20,w} = \frac{M(1 - \bar{v}\rho)}{Nf} \quad (1)$$

where  $M$  is the weight-average molecular mass,  $\bar{v}$  is the partial specific volume of GR,  $\rho$  is the solvent density, and  $N$  is Avogadro's number. The density was calculated from the buffer composition and temperature,<sup>11</sup> and the partial specific volume was calculated by summing the partial specific volume of each amino acid (0.7223 mL/g at 4 °C).<sup>12</sup>

For sedimentation equilibrium, three GR samples at 9.3, 4.2, and 0.9  $\mu$ M were equilibrated at 4 °C, using rotor speeds of 15000, 18000, and 21000 rpm. Samples were judged to be at equilibrium by successive subtraction of scans. All data were analyzed using nonlinear least-squares (NLLS) parameter estimation as implemented in NONLIN.<sup>13</sup> NONLIN uses the following equation to resolve the reduced molecular mass ( $\sigma$ ):

$$Y_r = \delta + \alpha \exp\left(\sigma \frac{r^2 - r_0^2}{2}\right) \quad (2)$$

where  $Y_r$  is the absorbance at radius  $r$ ,  $\delta$  is the baseline offset, and  $\alpha$  is the absorbance at the reference radius,  $r_0$ . The reduced molecular mass,  $\sigma$ , is defined as

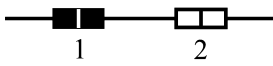
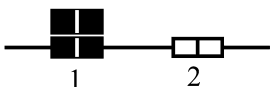
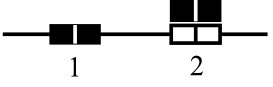
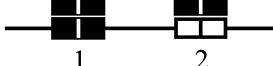
$$\sigma = \frac{M(1 - \bar{v}\rho)\omega^2}{RT} \quad (3)$$

where  $M$  is the weight-average molecular mass,  $\bar{v}$  is the partial specific volume of GR,  $\rho$  is the solvent density (calculated from the buffer composition and experimental temperature),<sup>11</sup>  $\omega$  is the angular velocity,  $R$  is the gas constant, and  $T$  is the absolute temperature in kelvin.

**DNA Preparation for DNase I Footprinting.** A promoter vector containing two tandemly linked glucocorticoid response elements [GRE<sub>2</sub> (see Figure 1D)] was donated by K. Horwitz (University of Colorado Anschutz Medical Center). Each GRE corresponds to an imperfect palindrome derived from the tyrosine aminotransferase promoter, TGTACAG-GATGTTCT,<sup>14</sup> spaced 25 bp apart. A reduced-valency template (GRE<sub>1-</sub>) containing a G-to-T point mutation in each half-site of the distal GRE (designated as site 1) was created in house. Each template was excised from its respective vector using *Hind*III and *Aat*II to generate a 1 kb promoter fragment and end-labeled with <sup>32</sup>P using a Klenow fill-in reaction. The proximal GRE of each fragment (site 2) was positioned 100 bp from the 3' end of the labeled strand. The sequence of the GRE<sub>2</sub> promoter is identical to that of the PRE<sub>2</sub> promoter used in our earlier work on the two PR isoforms<sup>5,6</sup> and differs only in response element sequence when compared to that of the ERE<sub>2</sub> promoter used in our work on ER- $\alpha$ .<sup>7</sup>

**Individual Site Binding Experiments.** Experiments were conducted using quantitative DNase I footprint titrations as originally described by Ackers and co-workers<sup>15,16</sup> with minor modifications.<sup>17</sup> All reactions were conducted in an assay buffer containing 20 mM Hepes (pH 8.0), 100 mM NaCl, 1 mM DTT, 1 mM CaCl<sub>2</sub>, 2.5 mM MgCl<sub>2</sub>, 10  $\mu$ M TA, 100  $\mu$ g/mL BSA, and 2  $\mu$ g/mL salmon sperm DNA. Each reaction mixture contained 15000 cpm of freshly labeled DNA. GR was added to each reaction mix, covering a concentration range from subnanomolar to low micromolar. Because GR reaches micromolar concentrations in the footprint titration, the concentrated receptor stock was dialyzed into the assay buffer without BSA and salmon sperm DNA prior to equilibration with promoter DNA. Samples were allowed to equilibrate at 4

Table 1. Species Distributions, Binding Constants, and Free Energy Changes for GR Assembly on the GRE<sub>2</sub> Promoter<sup>a</sup>

Species Number	Species Schematic	Macroscopic constant	Free Energy Contribution
1		--	reference state
2		$K_{\text{tot}}$	$\Delta G_{\text{tot}}$
3		$K_{\text{tot}}$	$\Delta G_{\text{tot}}$
4		$K_{\text{tot}}^2 \cdot k_{\text{c,inter}}$	$2 \cdot \Delta G_{\text{tot}} + \Delta G_{\text{c,inter}}$

<sup>a</sup>The free energy change is related to each macroscopic association constant through the relationship  $\Delta G_i = -RT \ln k_i$ , where  $R$  is the gas constant and  $T$  is the temperature in kelvin.

°C for at least 1 h. DNase I (Invitrogen) was diluted to a concentration of 0.025 unit/ $\mu\text{L}$  using the assay buffer without BSA and salmon sperm DNA. Five microliters of the diluted DNase I solution was added to each 100  $\mu\text{L}$  sample, and the reaction was allowed to proceed for exactly 2 min. Digestion products were electrophoresed on 6% acrylamide–urea gels and visualized using phosphorimaging. Individual site binding isotherms were calculated as described by Brenowitz et al.<sup>16</sup> using ImageQuant (Molecular Dynamics).

The thermodynamic validity of the quantitative DNase footprint titration technique is based upon the testable assumptions that the system of interest is at equilibrium and the DNase exposure does not perturb that equilibrium.<sup>16</sup> In this study, the resolved binding isotherms were independent of equilibration times from 1 to 2 h. All studies were conducted with DNase concentrations low enough to ensure “single-hit kinetics” and therefore thermodynamically valid binding isotherms.<sup>15</sup> Finally, promoter DNA concentrations (maximally 10 pM) were estimated to be well below the estimated GR DNA binding affinity, thus justifying the assumption that  $\text{GR}_{\text{free}} \approx \text{GR}_{\text{total}}$ .

#### Resolution of Microscopic Interaction Free Energies.

The DNase I footprint titration technique resolves the fractional occupancy of GR binding at each response element site. The statistical thermodynamic expressions that describe the individual site binding isotherms are constructed by summing the probabilities of each microscopic configuration that contributes to binding at that site. A detailed approach for generating each mathematical formulation has been presented previously.<sup>18</sup> Briefly, the probability ( $f_s$ ) of any microscopic configuration is defined as<sup>19</sup>

$$f_s = \frac{e^{(-\Delta G_s/RT)} x^j}{\sum_{s=1}^j e^{(-\Delta G_s/RT)} x^j} \quad (4)$$

where  $\Delta G_s$  is the free energy of configuration state  $s$  relative to that of the unliganded reference state,  $x$  is the free GR monomer concentration, and  $j$  is the stoichiometry of GR monomers bound to a response element.  $R$  is the gas constant, and  $T$  is the temperature in kelvin. The relationship between each free energy change and its association constant is described by the equation  $\Delta G_i = -RT \ln k_i$ .

The GRE<sub>1</sub> binding isotherms were first analyzed using the model-independent Hill equation:

$$\bar{Y}_{\text{Hill}} = \frac{x^n}{K^n + x^n} \quad (5)$$

where  $\bar{Y}_{\text{Hill}}$  is the fractional saturation at the response element,  $x$  is the free GR monomer concentration, and  $K$  is an apparent dissociation constant. This analysis yielded a Hill coefficient ( $n$ ) statistically indistinguishable from 2, indicative of strong cooperativity between adjacently bound monomers at a palindrome (see Results). Thus, the singly ligated monomer GR–DNA species is not significantly populated, and the affinity for monomer half-site binding is not well-constrained. All isotherms were therefore analyzed using a contracted Adair equation to resolve the total binding affinity ( $K_{\text{tot}}$ ) for assembling two GR monomers at a palindromic response element (Table 1). For the GRE<sub>1</sub> data sets, the following equation was used:

$$\bar{Y}_{\text{GRE}_1} = \frac{K_{\text{tot}} x^2}{1 + K_{\text{tot}} x^2} \quad (6)$$

where  $x$  is the free GR monomer concentration and  $K_{\text{tot}}$  is as described in Figure 1B.

For the GRE<sub>2</sub> data sets, eq 7 describes binding to both sites 1 and 2 of the GRE<sub>2</sub> promoter. Because the two sites are identical (Figure 1D),  $K_{\text{tot}}$  is assumed to be the same for each GRE. An additional term,  $k_{\text{c,inter}}$ , was included to describe potential cooperativity between the palindromes:

$$\bar{Y}_{\text{GRE}_2} = \frac{K_{\text{tot}} x^2 + K_{\text{tot}}^2 k_{\text{c,inter}} x^4}{1 + 2K_{\text{tot}} x^2 + K_{\text{tot}}^2 k_{\text{c,inter}} x^4} \quad (7)$$

The GRE<sub>2</sub> and GRE<sub>1</sub> data sets were then globally fit to resolve  $K_{\text{tot}}$  and  $k_{\text{c,inter}}$ .

Finally, because protein interactions at DNA binding sites do not afford complete protection from DNase activity, binding data were treated as transition curves fitted to upper ( $m$ ) and lower ( $b$ ) end points:

$$\bar{Y}_{\text{app}} = (m - b) \bar{Y} + b \quad (8)$$

Analyses of binding isotherm data were conducted with Scientist (Micromath, Inc.).



## RESULTS

Full-length human GR (both His- and FLAG-tagged) was purified from baculovirus-infected Sf9 insect cells using three chromatographic steps. For His-GR, densitometric analysis of Coomassie Blue-stained SDS-PAGE gels indicated that the receptor was at least 95% pure (Figure 2A). Mass spectrometry

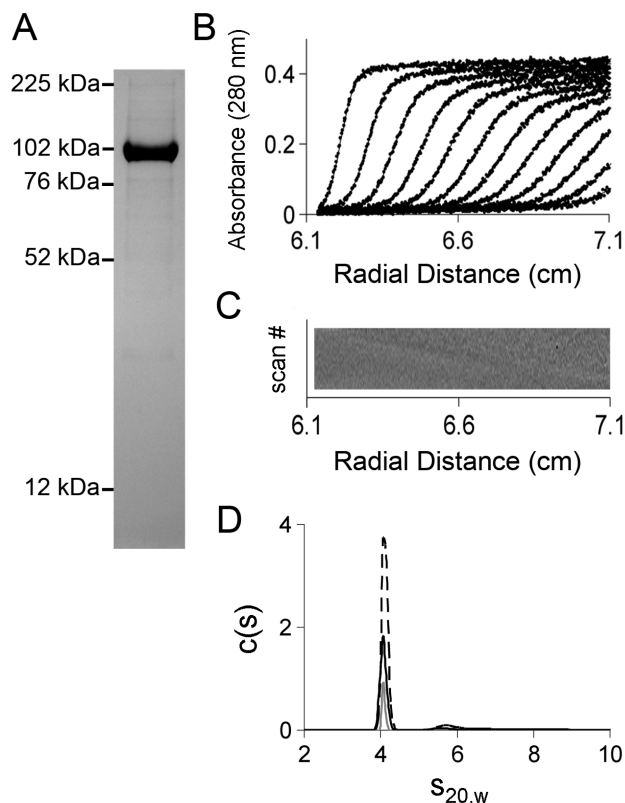


**Figure 2.** Purification of full-length human GR and analysis by sedimentation velocity. (A) Baculovirus-expressed GR was purified as described in Materials and Methods. The purified protein (8  $\mu$ g) was resolved by 4 to 12% gradient SDS-PAGE and Coomassie-stained. Molecular mass markers are indicated at the left. (B) Sedimentation velocity data collected using 5  $\mu$ M GR, at 100 mM NaCl, pH 8.0, and 4  $^{\circ}$ C. Filled circles represent the individual data points from scans taken at 50000 rpm, plotted as a function of time and radial position. Solid lines represent the best fit from a  $c(s)$  analysis as implemented by Sedfit.<sup>9</sup> Only every eighth scan is shown for the sake of clarity. (C) Residuals of the fits as represented by bitmap. Residuals are shown on a gray scale as a function of radius (x-axis) and scan number (y-axis). (D)  $c(s)$  distributions determined with Sedfit<sup>9</sup> for three GR concentrations: 10.0  $\mu$ M (---), 5.0  $\mu$ M (solid black line), and 2.0  $\mu$ M (solid gray line).

analysis of trypsin-digested His-GR resolved masses with the highest probability of corresponding to residues 5–777. The presence of the N-terminal His tag was confirmed by immunoblotting. FLAG-GR was purified to an identical degree and generated identical ultracentrifugation and DNase footprinting results, suggesting that the tags have little influence on receptor function.

**GR Is a Structurally Homogeneous Monomer.** Sedimentation velocity was used to examine the hydrodynamic and self-association properties of His-GR. These studies were conducted at concentrations ranging from 2.0 to 10.0  $\mu$ M. Figure 2B shows representative sedimentation velocity absorbance data, with the solid lines representing the best fit

via  $c(s)$  analysis as implemented in Sedfit.<sup>9</sup> The residuals of the fit, as represented by a bitmap, are shown in Figure 2C. Figure 2D shows the resolved sedimentation coefficient distributions for three GR concentrations. It is evident that regardless of concentration, the vast majority of GR sediments as a single species with a temperature- and buffer-corrected sedimentation coefficient ( $s_{20,w}$ ) of 4.1 S. A  $c(M)$  analysis of the 4.1 S peak resolved a molecular mass of 80407 Da, slightly less than the calculated monomer molecular mass of 90925 Da. We routinely observe a minor peak at 5.7 S, corresponding to a molecular mass of 159241 Da, and thus consistent with a GR dimer. However, the percentage of the dimer ( $\sim$ 7%) is always invariant with respect to receptor concentration, suggesting that it reflects an irreversible, functionally incompetent species. Thus, the velocity results indicate that contrary to dogma, ligand-bound GR exists almost exclusively in a monomeric state. An identical result was observed regardless of salt concentration and pH (data not shown).

Sedimentation equilibrium was used to directly measure the molecular mass of the putative monomer species observed in the velocity studies. We conducted sedimentation equilibrium studies at three GR concentrations (9.3, 4.2, and 0.9  $\mu$ M) and three rotor speeds (15000, 18000, and 21000 rpm), using buffer conditions identical to those used in the velocity studies. Global fitting of the nine data sets to a single-species model resolved an average molecular mass of  $96400 \pm 3400$  Da, slightly above that of a GR monomer ( $SD_{fit} = 0.0033$  AU). Analyses using more complex interaction models (e.g., monomer–dimer equilibrium) offered no improvement in the fit. However, because the velocity data detected a larger, noninteracting species consistent with that of a dimer, we also fit the equilibrium data to a model allowing for two noninteracting species. Shown in Figure 3 are the results of that analysis. It is evident that the noninteracting, two-species model describes well all the data ( $SD_{fit} = 0.0024$  AU). Moreover, the resolved molecular mass of the monomer species is  $87972 \pm 2900$  Da, within 3% of the calculated molecular mass of the monomer. Finally, the resolved stoichiometry from the two species fit was determined to be  $2.0 \pm 0.4$ , strongly suggesting that the larger sedimenting species is indeed the GR dimer. Consistent with this, fitting of the individual data sets to a monomer–dimer model resolved binding constants that became weaker with an increasing receptor concentration. Thus, the ratio of monomer to dimer was constant as a function of total protein concentration, indicative of an irreversible dimer species. We therefore conclude that GR is overwhelmingly monomeric with only a small population of incompetent, irreversible dimer.

Finally, the good agreement in molecular mass estimates between the velocity and equilibrium studies suggests that the GR monomer is structurally homogeneous, because even small amounts of structural heterogeneity (e.g., incompetent dimer) tend to dramatically underestimate molecular mass estimates when determined by sedimentation velocity.<sup>9,20</sup> If GR is indeed a homogeneous monomer, this allows for a number of physically meaningful hydrodynamic calculations. For example, the monomer has a Stokes radius of 54 Å and a frictional ratio of 1.59, indicative of significant asymmetry. Thus, if modeled as a prolate ellipsoid, GR has a major:minor axial ratio of 11:1. These results are summarized in Table 2.

**GR Assembles at a Two-Site Promoter with Substantial Cooperativity.** Quantitative DNase footprint titrations were used to resolve the energetics of GR assembly at a

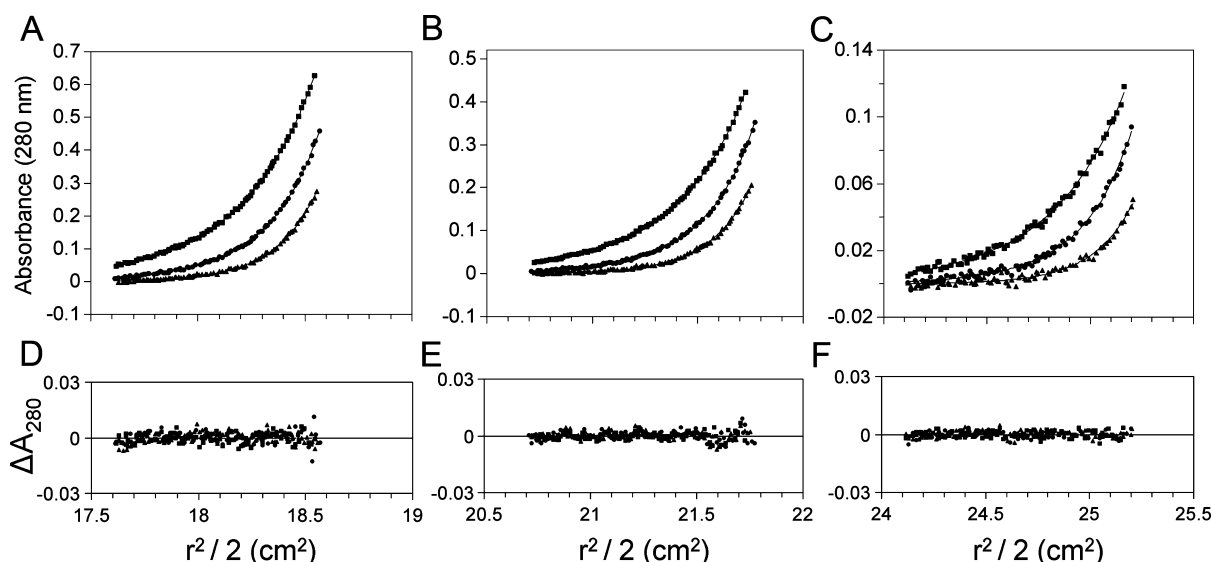


**Figure 3.** Sedimentation equilibrium analysis of GR, plotted as absorbance vs  $r^2/2$ . (A–C) Sedimentation equilibrium data for GR at three different initial loading concentrations: 9.3 (A), 4.2 (B), and 0.9  $\mu\text{M}$  (C). Symbols represent GR absorbance at 15000 (■), 18000 (●), and 21000 rpm (▲). Solid lines represent simultaneous analysis of all nine data sets to a noninteracting, two-species model. The square root of variance was 0.0024 absorbance unit. (D–F) Residuals from the two-species model plotted as the change in absorbance vs  $r^2/2$  for initial loading concentrations of 9.3 (D), 4.2 (E), and 0.9  $\mu\text{M}$  (F).

**Table 2. Hydrodynamic Properties of GR**

$s_{20,w}$	4.1
$f$ (g/s)	$1.03 \times 10^{-7}$
$f/f_0$	1.59
Stokes radius (Å)	54
axial ratio	11:1
molecular mass (Da) <sup>a</sup>	80407
molecular mass (Da) <sup>b</sup>	$87972 \pm 2900$

<sup>a</sup>Estimated by a  $c(M)$  analysis of the 4.1 S peak as implemented in Sedfit. <sup>b</sup>Resolved molecular mass from sedimentation equilibrium.

promoter containing two palindromic response elements (GRE<sub>2</sub>). Shown in Figure 4A is a representative titration of the GRE<sub>2</sub> promoter under buffer conditions identical to those of the sedimentation studies. It is evident that GR binding is highly specific, and sequencing studies confirm that the protected regions correspond to the two GREs. Receptor-induced DNase hypersensitivity adjacent to the response elements is also evident. This was seen in our earlier work on ER- $\alpha$  and the two PR isoforms<sup>5–7</sup> and has been previously attributed to receptor-induced DNA bending.<sup>21,22</sup>

Our standard approach to quantifying steroid receptor–promoter interactions has been to independently determine receptor dimerization affinity ( $k_{di}$ ) and then to fix this value in a global nonlinear least-squares analysis of the individual site binding isotherms to resolve the intrinsic ( $k_{int,d}$ ) and intersite cooperative ( $k_{c,inter}$ ) binding constants (Figure 1B).<sup>5–7</sup> Such an analysis resolves the microscopic energetics of response element binding using a model that assumes preformed dimers bind to the palindromic response elements. However, because we found no evidence of reversible self-association of the receptor, this approach was not ideal. Attempts to fit the data using a sequential monomer binding model were also unsuccessful. This was due to the strong DNA-induced cooperativity known to exist between adjacently bound GR monomers.<sup>23</sup> Consistent with this, fitting the single response

element GRE<sub>1</sub> isotherms to a model-independent Hill equation resolved an  $n$  of  $2.2 \pm 0.2$ .

We therefore globally fit the individual site binding isotherms (Figure 4B) to a contracted Adair equation (eqs 6 and 7). This approach allowed us to resolve the total affinity for loading two GR monomers on a single palindromic sequence ( $K_{tot}$ ), and the extent of GR cooperativity between adjacent palindromic sites ( $k_{c,inter}$ ). Using this approach, we find that GR assembles at a palindromic response element with a  $K_{tot}$  of  $5.18 \times 10^{13} \text{ M}^{-2}$ . This corresponds to a binding free energy of  $-17.4 \text{ kcal/mol}$  and an apparent dissociation constant of 140 nM or  $-8.7 \text{ kcal/mol}$ .<sup>24</sup>

The intersite cooperativity ( $k_{c,inter}$ ) associated with binding the GRE<sub>2</sub> promoter was determined to be  $69 \pm 20$ , which corresponds to a free energy of  $-2.3 \text{ kcal/mol}$ . Consistent with this, global fitting of the GRE<sub>2</sub> binding isotherms to the Hill equation resolved an  $n$  of  $2.5 \pm 0.1$ . The increase in  $n$  above that reported for the GRE<sub>1</sub> template is consistent with the moderate to strong cooperativity associated with fully loading the GRE<sub>2</sub> promoter. All binding parameters and their associated errors are summarized in Table 3. Finally, the standard deviation for the global fit was 0.068 fractional saturation unit.

## DISCUSSION

**Cooperative Binding Energetics of GR.** Previous biochemical studies of GR have used either isolated domains or partially purified holoproteins.<sup>14,23,25,26</sup> This study represents the first dissection of GR–promoter energetics using the highly purified and rigorously characterized full-length receptor. Using analytical ultracentrifugation to determine the GR self-assembly state, we found that GR exists as a structurally homogeneous monomer at protein concentrations of at least 10  $\mu\text{M}$ . Using quantitative footprinting to measure GR–promoter binding energetics, we found that GR assembles at a multisite promoter with strong binding affinity and with significant intersite cooperativity.

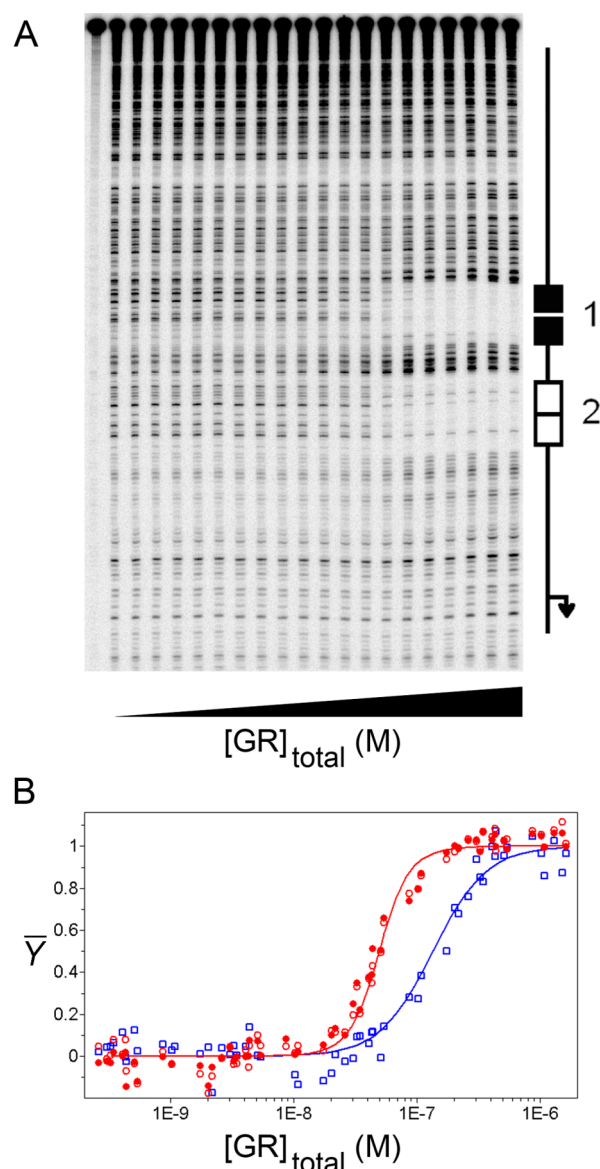


**Figure 4.** Quantitative DNase footprint titrations and individual site binding isotherms determined from global analysis of the GRE<sub>1</sub>- and GRE<sub>2</sub> promoters. (A) Representative DNase footprint titration image of binding of GR to the GRE<sub>2</sub> promoter in 100 mM NaCl. The GR concentration increases from left to right. Positions of the two GREs (site 1, filled rectangle; site 2, empty rectangle) are indicated at the right. (B) Individual site binding isotherms generated from analysis of the footprint titration images. Filled red circles represent binding to site 1, and empty red circles represent binding to site 2 of the GRE<sub>2</sub> promoter (three independent footprint titrations); empty blue squares represent binding to the GRE<sub>1</sub>- promoter (three independent footprint titrations). The red and blue lines represent the best global fits to all binding isotherms using the macroscopic binding model described by eqs 6 and 7. The sequences are identical for both sites of the GRE<sub>2</sub> promoter; thus, the fit lines for sites 1 and 2 overlay.

**Table 3. Resolved Free Energy Changes (kilocalories per mole) for GR–GRE<sub>2</sub> Binding Interactions<sup>a</sup>**

$\Delta G_{di}$	$\geq -5.1$
$\Delta G_{tot}$	$-17.4 \pm 0.1$
$\Delta G_{c,inter}$	$-2.3 \pm 0.2$

<sup>a</sup>Errors correspond to 67% confidence intervals.

With regard to GR self-association, because sedimentation analyses are capable of detecting at least 10% dimer, the dimerization constant of GR must be no stronger than 100  $\mu$ M (if it is even capable of dimerizing). Our results thus contradict earlier semiquantitative studies indicating that GR dimerizes with nanomolar affinity<sup>25,26</sup> and raise questions about the physiological relevance of the dimeric GR hormone binding domain observed by crystallographic analysis.<sup>27</sup> The origins of these differences are unclear; however, we note that biochemical estimates of GR dimerization used either a partially purified receptor derived from animal tissue<sup>25</sup> or an unpurified receptor generated by recombinant expression.<sup>26</sup> With regard to the crystallographic results, GR dimerization may have been induced by the high concentration of protein needed for crystallization. Alternatively, the dimeric state may be a consequence of crystal packing or nonphysiological buffer conditions. Nonetheless, despite these discrepancies, the hydrodynamic asymmetry seen in our sedimentation velocity studies (thus indicative of a nonglobular GR structure) is entirely consistent with the natively unfolded N-terminal regions known to exist for GR and other receptors.<sup>28–31</sup>

**Comparison to Homologous Receptors.** Plotted in Figure 5 are the microstate interaction energetics for binding of

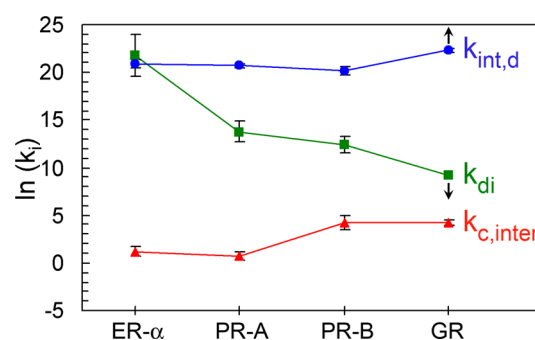


**Figure 5.** Distribution of microscopic promoter binding affinities for assembly of ER- $\alpha$ , PR-A, PR-B, and GR dimer at a two-site promoter. Individual constants are denoted as follows. Blue circles represent preformed dimer binding affinity ( $k_{int,d}$ ). Green squares represent receptor dimerization affinity ( $k_{di}$ ). Red triangles represent intersite cooperativity ( $k_{c,inter}$ ). Error bars represent 67% confidence intervals. All parameters were determined under identical solution conditions using either a PRE<sub>2</sub> promoter<sup>5,7</sup> or an ERE<sub>2</sub> promoter.<sup>7</sup> Arrows associated with the  $k_{di}$  or  $k_{int,d}$  parameters of GR indicate that these values can only decrease or increase, respectively, because the minimal assumed dimerization constant of 100  $\mu$ M can become only weaker.

PR-A, PR-B, and GR to the promoter sequence shown in Figure 1D. Also shown are the microstate interaction energetics for binding of ER- $\alpha$  to a promoter that differs only in response element sequence.<sup>7</sup> All parameters were determined using highly purified receptor preparations analyzed under conditions identical to those used here.<sup>5–7</sup> The energetics for ER- $\alpha$  and the two PR isoforms were determined using the well-accepted dimer binding model in which receptors dimerize in the absence of DNA ( $k_{di}$ ) and only the preformed dimers assemble at DNA binding sites ( $k_{int,d}$ ). For comparative purposes, we therefore fit the GR footprinting data to the same model assuming the strongest possible dimerization constant consistent with our sedimentation data (100  $\mu$ M). Interestingly, such a fit reports an intrinsic binding affinity ( $k_{int,d}$ ) for GR dimer binding of 0.2 nM, comparable to the nanomolar affinities of ER- $\alpha$ , PR-A, and PR-B.<sup>5–7</sup> This concordance



suggests that if GR dimerizes in the absence of DNA, the dimerization affinity is unlikely to be significantly weaker than 100  $\mu\text{M}$ , because that would greatly increase the intrinsic binding affinity. Finally, the dimer binding model resolved a GR intersite cooperativity term of  $-2.3$  kcal/mol, unchanged from the Adair fit.

Visual inspection makes it clear that all the receptors maintain similar intrinsic dimer binding affinities ( $k_{\text{int,d}}$ ). This is not surprising because the receptor DNA binding domains are highly conserved by sequence and are structurally similar as determined by crystallographic analysis.<sup>32–34</sup> By contrast, the dimerization energetics ( $k_{\text{di}}$ ) vary dramatically. For example, the nanomolar dimerization affinity seen for ER- $\alpha$  is  $\sim 1000$ -fold stronger than that of the two PR isoforms, and at least 100000-fold stronger than that of GR. The intersite cooperative binding energetics ( $k_{\text{c,inter}}$ ) also vary significantly. For example, ER- $\alpha$  and PR-A show essentially no cooperativity, whereas both PR-B and GR exhibit strong cooperative stabilization of  $\sim 70$ -fold. Although cooperativity varies much less than that seen for dimerization, this does not diminish its importance; it is well established that only small changes in cooperative energetics generate dramatic functional consequences for genetic switching mechanisms.<sup>18</sup>

**Functional Implications of Differential Promoter Binding Energetics.** As noted in the introductory section, we are focused on determining the quantitative principles responsible for specificity of steroid receptor-mediated gene regulation. In particular, we are interested in the basis of the functional specificity in the face of competitive DNA binding by homologous receptors. Here we attempt to model different competitive binding scenarios that might occur in vivo. We speculate that the large differences in microstate binding energetics seen in Figure 5 serve as the basis for generating receptor-specific and promoter-specific gene regulation. Here we use PR-B and GR as an example; both receptors are strong transcriptional activators yet are capable of activating overlapping but distinct gene networks.<sup>4</sup> The two proteins thus serve as a model system for exploring possible mechanisms of specificity in steroid receptor function.

Shown in Figure 6 are the calculated probabilities of the fully ligated state (e.g., the presumptive transcriptionally active microstate) for GR and PR-B assembly at various promoter layouts, using the experimentally determined binding energetics determined here and in ref 7. We simulated both noncompetitive and competitive binding of the receptor to the promoters. In the noncompetitive binding scenario (Figure 6A), each receptor is allowed to assemble at the promoter in the absence of the other. In the competitive binding scenarios (Figure 6B–D), the receptors compete for binding sites, assuming that both exist at equimolar concentrations at all points along the simulation. (The equations used for all simulations are presented in the Supporting Information.) It is clear that the probability and half-saturation values of the fully ligated (i.e., transcriptionally active) microstate are similar for both receptors. This is the case regardless of whether one assumes that the receptors bind DNA as preformed dimers or by successive monomer binding, thus suggesting that the binding pathway (successive monomer vs preformed dimer) is unimportant in receptor function. However, shown in Figure 6B is the same simulation now under competitive binding conditions. To better illustrate how dimerization energetics influence promoter occupancy, we assumed that preformed PR-B and GR dimers compete for DNA binding with identical

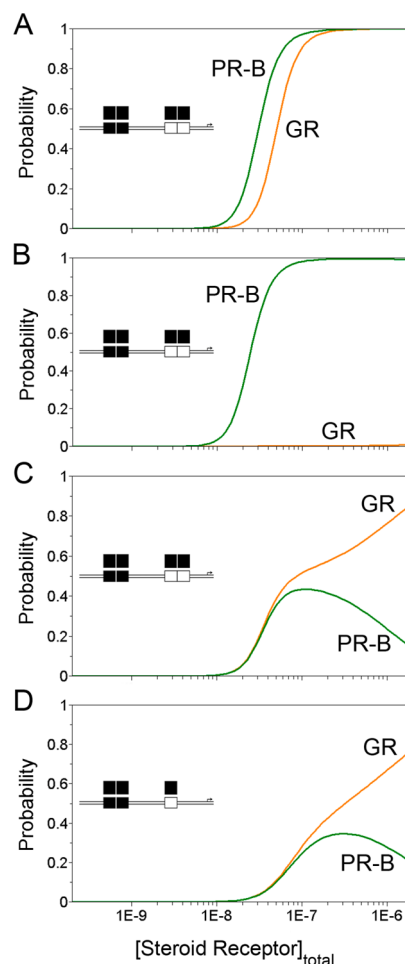


**Figure 6.** Predicted probabilities of the fully ligated promoter state when bound by either PR-B or GR. (A) Simulation of noncompetitive binding of PR-B (green line) and GR (orange line) to the GRE<sub>2</sub> promoter using the experimentally determined  $K_{\text{tot}}$  values. (B) Simulation of competitive binding of PR-B and GR to the GRE<sub>2</sub> promoter assuming both receptors bind via a dimer binding pathway. Simulations were conducted using dimerization constants of 4.3 and 100  $\mu\text{M}$  for PR-B and GR, respectively; intrinsic binding affinities were kept identical. Heterologous promoter occupancy (e.g., PR-B and GR dimers occupying an identical promoter) was not considered because there is no evidence to support this assumption. (C) Simulation of competitive binding of PR-B and GR to the GRE<sub>2</sub> promoter assuming both receptors bind the promoter via a monomer binding pathway. Simulations were conducted using dimerization constants of 4.3 and 100  $\mu\text{M}$  for PR-B and GR, respectively; identical intrasite cooperativity terms ( $k_{\text{c,intra}}$ ) of 1000; and the assumption that monomer affinity ( $k_{\text{int,m}}$ ) was identical for both half-sites within a palindrome. (D) Simulation of competitive binding of PR-B and GR to a promoter containing a single response element and an adjacent half-site, assuming both receptors bind the promoter using a monomer binding pathway and assumptions described for panel C.

intrinsic binding affinities (0.8 nM) and intersite cooperative affinities ( $k_{\text{c,inter}} = 70$ ); thus, the only difference is in dimerization affinity (4.3  $\mu\text{M}$  for PR-B vs 100  $\mu\text{M}$  for GR). Clearly, PR-B easily outcompetes GR for binding. This is simply because the stronger dimerization energetics of PR-B generate a greater dimer population (i.e., active binding species) relative to GR at identical total protein concentrations. Thus, receptor-specific promoter occupancy, and perhaps receptor-specific gene regulation, may be generated even if



both receptors exhibit identical intrinsic DNA binding affinities for the promoter.

Shown in Figure 6C is the same simulation that is shown in Figure 6B, but now assuming that PR-B and GR bind as successive monomers to the promoter. Monomer binding affinities were determined as follows. (1) PR-B and GR binding isotherms were fit to a monomer binding model using dimerization constants of 4.3 and 100  $\mu\text{M}$ , respectively. (2) Identical intrasite cooperativity terms ( $k_{c,\text{intra}}$ ) of 1000 were assumed. (3) The monomer binding affinity ( $k_{\text{int},m}$ ) was assumed to be identical for both half-sites within a single response element. Using these assumptions, similar monomer binding affinities and intersite cooperativity values were resolved for the two receptors (data not shown). We then conducted the simulations assuming that  $k_{\text{int},m}$ ,  $k_{c,\text{intra}}$ , and  $k_{c,\text{inter}}$  were identical; thus, the only difference between the receptors was again the difference in dimerization affinity ( $k_{\text{di}}$ ). We now see that GR effectively competes for binding at lower protein concentrations and eventually outcompetes PR-B at higher concentrations. In this case, the concentration of assumed DNA binding species (monomer) is decreased for PR-B because of its stronger dimerization energetics. These results point out the importance of determining the rules and states associated with receptor assembly at a promoter; depending upon the pathway, a promoter may be preferentially bound by one receptor (Figure 6B) or competitively bound by both receptors (Figure 6C). Finally, the simulations emphasize the need for kinetic studies to determine the extent to which steroid receptors follow successive monomer versus preformed dimer binding pathways.

Finally, shown in Figure 6D is a different promoter layout consisting of a combination of a palindromic and a half-site response element. This type of architecture is seen in natural PR- and GR-regulated promoters such as MMTV<sup>35</sup> and in genome-wide computational analyses of receptor binding sites.<sup>36</sup> Using a monomer binding model for both PR-B and GR, we see that the receptors equally compete for binding until receptor concentrations reach supraphysiological levels. At these concentrations, GR begins to dominate the binding because of its weaker dimerization constant and thus larger monomer population. Thus, differences in promoter layout, as well as microstate energetics, lead to different outcomes in receptor-specific promoter occupancy.

In summary, combining different microstate energetics with different promoter architectures predicts PR-B-dominated binding in one scenario (Figure 6B) and competitive PR-B and GR binding in a second (Figure 6C,D). Moreover, promoter occupancy is initiated at the tens of nanomolar receptor concentrations thought to exist intracellularly.<sup>37</sup> We note that the parameter that differs most between PR-B and GR is dimerization affinity; however, differences in intersite cooperativity as seen between the PR isoforms and ER- $\alpha$  should allow even greater specificity of promoter occupancy. These results therefore suggest a quantitative framework for considering receptor-specific and promoter-specific gene regulation. It may eventually be possible to predict the receptor-specific transcriptional behavior of natural promoters or design synthetic promoter architectures capable of receptor-specific gene activation, even when multiple receptors are present and active.

## ■ ASSOCIATED CONTENT

### § Supporting Information

In Figure 6, we simulate the probability of the fully ligated state for assembly of GR and PR-B at various promoter layouts. The equations necessary for modeling the different competitive binding scenarios are given in the Supporting Information. This material is available free of charge via the Internet at <http://pubs.acs.org>.

## ■ AUTHOR INFORMATION

### Corresponding Author

\*Department of Pharmaceutical Sciences, C-238 University of Colorado Anschutz Medical Campus, 12850 E. Montview Blvd., Aurora, CO 80045. Phone: (303) 724-6118. Fax: (303) 724-7266. E-mail: [david.bain@ucdenver.edu](mailto:david.bain@ucdenver.edu).

### Funding

This work was supported by National Institutes of Health Grants DK61933 and DK88843 and the Avon Foundation for Women (D.L.B.). J.P.R. was supported by National Research Service Award Training Fellowship DK897922.

### Notes

The authors declare no competing financial interest.

## ■ ACKNOWLEDGMENTS

We thank Dr. N. Karl Maluf and Dr. Keith D. Connaghan for critical discussions. We thank Ms. Fran Crawford and the Kapplar/Marrack Laboratory (National Jewish Medical and Research Center, Denver, CO) for assistance and training in insect cell/baculovirus protein expression systems.

## ■ ABBREVIATIONS

AR, androgen receptor; ER- $\alpha$ , estrogen receptor  $\alpha$  isoform; ER- $\beta$ , estrogen receptor  $\beta$  isoform; GR, glucocorticoid receptor; MR, mineralocorticoid receptor; PR, progesterone receptor; PR-A, progesterone receptor A isoform; PR-B, progesterone receptor B isoform; DBD, DNA binding domain; HBD, hormone binding domain; AF, activation function; TA, triamcinolone acetonide; DTT, dithiothreitol;  $\beta$ -ME, 2-mercaptoethanol; GRE, glucocorticoid response element; HRE, hormone response element; PRE, progesterone response element; MMTV, mouse mammary tumor virus.

## ■ REFERENCES

- (1) Tsai, M. J., and O'Malley, B. W. (1994) Molecular mechanisms of action of steroid/thyroid receptor superfamily members. *Annu. Rev. Biochem.* 63, 451–486.
- (2) Monroe, D. G., Getz, B. J., Johnsen, S. A., Riggs, B. L., Khosla, S., and Spelsberg, T. C. (2003) Estrogen receptor isoform-specific regulation of endogenous gene expression in human osteoblastic cell lines expressing either ER $\alpha$  or ER $\beta$ . *J. Cell. Biochem.* 90, 315–326.
- (3) Richer, J. K., Jacobsen, B. M., Manning, N. G., Abel, M. G., Wolf, D. M., and Horwitz, K. B. (2002) Differential gene regulation by the two progesterone receptor isoforms in human breast cancer cells. *J. Biol. Chem.* 277, 5209–5218.
- (4) Wan, Y., and Nordeen, S. K. (2002) Overlapping but distinct gene regulation profiles by glucocorticoids and progestins in human breast cancer cells. *Mol. Endocrinol.* 16, 1204–1214.
- (5) Connaghan-Jones, K. D., Heneghan, A. F., Miura, M. T., and Bain, D. L. (2007) Thermodynamic analysis of progesterone receptor-promoter interactions reveals a molecular model for isoform-specific function. *Proc. Natl. Acad. Sci. U.S.A.* 104, 2187–2192.
- (6) Heneghan, A. F., Connaghan-Jones, K. D., Miura, M. T., and Bain, D. L. (2006) Cooperative DNA binding by the B-isoform of

human progesterone receptor: Thermodynamic analysis reveals strongly favorable and unfavorable contributions to assembly. *Biochemistry* 45, 3285–3296.

(7) Moody, A. D., Miura, M. T., Connaghan, K. D., and Bain, D. L. (2012) Thermodynamic dissection of estrogen receptor-promoter interactions reveals that steroid receptors differentially partition their self-association and promoter binding energetics. *Biochemistry* 51, 739–749.

(8) Gill, S. C., and von Hippel, P. H. (1989) Calculation of protein extinction coefficients from amino acid sequence data. *Anal. Biochem.* 182, 319–326.

(9) Schuck, P. (2000) Size-distribution analysis of macromolecules by sedimentation velocity ultracentrifugation and Lamm equation modeling. *Biophys. J.* 78, 1606–1619.

(10) van Holde, K. E. (1985) *Physical Biochemistry*, 2nd ed., Prentice-Hall, Englewood Cliffs, CA.

(11) Laue, T. M., Shah, B. D., Ridgeway, T. M., and Pelletier, S. L. (1992) *Analytical Ultracentrifugation in Biochemistry and Polymer Science*, Royal Society of Chemistry, Cambridge, U.K.

(12) Cohn, E. J., and Edsall, J. T. (1943) *Proteins, Amino Acids, and Peptides*, Reinhold, New York.

(13) Johnson, M. L., Correia, J. J., Yphantis, D. A., and Halvorson, H. R. (1981) Analysis of data from the analytical ultracentrifuge by nonlinear least-squares techniques. *Biophys. J.* 36, 575–588.

(14) Jantzen, H. M., Strahle, U., Gloss, B., Stewart, F., Schmid, W., Boshart, M., Miksicsek, R., and Schutz, G. (1987) Cooperativity of glucocorticoid response elements located far upstream of the tyrosine aminotransferase gene. *Cell* 49, 29–38.

(15) Brenowitz, M., Senear, D. F., Shea, M. A., and Ackers, G. K. (1986) “Footprint” titrations yield valid thermodynamic isotherms. *Proc. Natl. Acad. Sci. U.S.A.* 83, 8462–8466.

(16) Brenowitz, M., Senear, D. F., Shea, M. A., and Ackers, G. K. (1986) Quantitative DNase footprint titration: A method for studying protein-DNA interactions. *Methods Enzymol.* 130, 132–181.

(17) Connaghan-Jones, K. D., Moody, A. D., and Bain, D. L. (2008) Quantitative DNase footprint titration: A tool for analyzing the energetics of protein-DNA interactions. *Nat. Protoc.* 3, 900–914.

(18) Ackers, G. K., Johnson, A. D., and Shea, M. A. (1982) Quantitative model for gene regulation by  $\lambda$  phage repressor. *Proc. Natl. Acad. Sci. U.S.A.* 79, 1129–1133.

(19) Hill, T. L. (1960) *An Introduction to Statistical Thermodynamics*, Dover Publications, New York.

(20) Philo, J. S. (2000) A method for directly fitting the time derivative of sedimentation velocity data and an alternative algorithm for calculating sedimentation coefficient distribution functions. *Anal. Biochem.* 279, 151–163.

(21) Nardulli, A. M., Greene, G. L., and Shapiro, D. J. (1993) Human estrogen receptor bound to an estrogen response element bends DNA. *Mol. Endocrinol.* 7, 331–340.

(22) Petz, L. N., Nardulli, A. M., Kim, J., Horwitz, K. B., Freedman, L. P., and Shapiro, D. J. (1997) DNA bending is induced by binding of the glucocorticoid receptor DNA binding domain and progesterone receptors to their response element. *J. Steroid Biochem. Mol. Biol.* 60, 31–41.

(23) Hard, T., Dahlman, K., Carlstedt-Duke, J., Gustafsson, J. A., and Rigler, R. (1990) Cooperativity and specificity in the interactions between DNA and the glucocorticoid receptor DNA-binding domain. *Biochemistry* 29, 5358–5364.

(24) Wyman, J., and Gill, S. J. (1990) *Binding and Linkage: Functional Chemistry of Biological Macromolecules*, University Science Books, Mill Valley, CA.

(25) Perlmann, T., Eriksson, P., and Wrangé, O. (1990) Quantitative analysis of the glucocorticoid receptor-DNA interaction at the mouse mammary tumor virus glucocorticoid response element. *J. Biol. Chem.* 265, 17222–17229.

(26) Segard-Maurel, I., Rajkowski, K., Jibard, N., Schweizer-Groyer, G., Baulieu, E. E., and Cadepond, F. (1996) Glucocorticosteroid receptor dimerization investigated by analysis of receptor binding to

glucocorticosteroid responsive elements using a monomer-dimer equilibrium model. *Biochemistry* 35, 1634–1642.

(27) Bledsoe, R. K., Montana, V. G., Stanley, T. B., Delves, C. J., Apolito, C. J., McKee, D. D., Consler, T. G., Parks, D. J., Stewart, E. L., Willson, T. M., Lambert, M. H., Moore, J. T., Pearce, K. H., and Xu, H. E. (2002) Crystal structure of the glucocorticoid receptor ligand binding domain reveals a novel mode of receptor dimerization and coactivator recognition. *Cell* 110, 93–105.

(28) Bain, D. L., Franden, M. A., McManaman, J. L., Takimoto, G. S., and Horwitz, K. B. (2000) The N-terminal region of the human progesterone A-receptor. Structural analysis and the influence of the DNA binding domain. *J. Biol. Chem.* 275, 7313–7320.

(29) Bain, D. L., Franden, M. A., McManaman, J. L., Takimoto, G. S., and Horwitz, K. B. (2001) The N-terminal region of human progesterone B-receptors: Biophysical and biochemical comparison to A-receptors. *J. Biol. Chem.* 276, 23825–23831.

(30) Baskakov, I. V., Kumar, R., Srinivasan, G., Ji, Y. S., Bolen, D. W., and Thompson, E. B. (1999) Trimethylamine N-oxide-induced cooperative folding of an intrinsically unfolded transcription-activating fragment of human glucocorticoid receptor. *J. Biol. Chem.* 274, 10693–10696.

(31) Hilser, V. J., and Thompson, E. B. (2011) Structural dynamics, intrinsic disorder, and allostery in nuclear receptors as transcription factors. *J. Biol. Chem.* 286, 39675–39682.

(32) Luisi, B. F., Xu, W. X., Otwinowski, Z., Freedman, L. P., Yamamoto, K. R., and Sigler, P. B. (1991) Crystallographic analysis of the interaction of the glucocorticoid receptor with DNA. *Nature* 352, 497–505.

(33) Roemer, S. C., Donham, D. C., Sherman, L., Pon, V. H., Edwards, D. P., and Churchill, M. E. (2006) Structure of the progesterone receptor-deoxyribonucleic acid complex: Novel interactions required for binding to half-site response elements. *Mol. Endocrinol.* 20, 3042–3052.

(34) Schwabe, J. W., Chapman, L., Finch, J. T., and Rhodes, D. (1993) The crystal structure of the estrogen receptor DNA-binding domain bound to DNA: How receptors discriminate between their response elements. *Cell* 75, 567–578.

(35) Connaghan-Jones, K. D., Heneghan, A. F., Miura, M. T., and Bain, D. L. (2008) Thermodynamic dissection of progesterone receptor interactions at the mouse mammary tumor virus promoter: Monomer binding and strong cooperativity dominate the assembly reaction. *J. Mol. Biol.* 377, 1144–1160.

(36) Jacobsen, B. M., Jambal, P., Schittone, S. A., and Horwitz, K. B. (2009) ALU repeats in promoters are position-dependent co-response elements (coRE) that enhance or repress transcription by dimeric and monomeric progesterone receptors. *Mol. Endocrinol.* 23, 989–1000.

(37) Theofan, G., and Notides, A. C. (1984) Characterization of the calf uterine progesterone receptor and its stabilization by nucleic acids. *Endocrinology* 114, 1173–1179.